Spaceborne Sensors Observe El Niño Teleconnection

W. Timothy Liu, Wenqing Tang, and Hua Hu
Jet Propulsion Laboratory
California Institute of Technology
Pasadena, CA 91109

The synoptic ocean surface wind field derived from the National Aeronautics and Space Administration (NASA) Scatterometer (NSCAT), with its superior spatial resolution [Liu et al., 1998], reveals that the three regions of simultaneous anomalous warming in the North Pacific Ocean observed at the end of May 1997 (Fig. 1) are related to wind anomalies through different mechanisms. The anomalous warming along the equator is part of the developing El Niño condition and is related to the westerly wind anomalies and the relaxation of the trade-winds over the equatorial Pacific. The equatorial westerly wind anomalies are connected to the anomalous cyclonic wind pattern in the northeast Pacific. The anomalous warming along the west coast of the United States is the result of the movement of a pre-existing pool of anomalously warm water with the cyclonic wind anomalies toward the coast. The warm pool is part of an anomalous sea surface temperature (SST) anomalies dipole which has been present for more than a year in the North Pacific; the warm pole is associated with warm and moist southerly winds and the cool pole with cool and dry northerly winds. The anomalous cyclonic circulation also causes anomalous southerly winds, suppression of coastal upwelling, and anomalous warming along the Mexican coast.

Fig. 1 shows positive SST anomalies along the entire central and eastern equatorial Pacific, from 1°C in the west to 4°C in the east, as part of a brewing El Niño. The strong equatorial westerly wind anomalies are clearly present in the central Pacific. Figs. 2a, 2b, and 2c, show time-longitude sections along the equator from Indonesia, across the Pacific, to the Galapagos. Wind blowing from west to east are positive (green to red) and wind blowing from east to west are negative (blue and purple). From the start of operation on September 15, 1996, NSCAT observed anomalous strong easterly trade-winds (4 m/s above normal) in the equatorial Pacific (Fig. 2a), which may have piled up warm water in the western Pacific, as reflected in 1°C positive SST (Fig. 2b), and 10 cm sea level (Fig. 2c) anomalies in the west. NSCAT observed a number of episodes of strong westerly wind anomalies in the central Pacific, including one in December-January and one in March. These wind anomalies generate downwelling Kelvin waves that propagate across the Pacific as positive sea-level anomalies [Liu, et al., 1995]. After the strong bursts of westerly wind anomalies in March, SST anomalies began to appear in the central and eastern equatorial Pacific. The sea level anomalies are larger than those generated earlier by Kelvin waves because of temperature increase. Except for a short period around May 15, 1996, the central equatorial Pacific was dominated by westerly anomalies, implying the collapse of the tradewinds and the depression of the thermocline, resulting in positive anomalies of SST and sea level. This appears to be the typical mechanism of equatorial anomalies associated with an El Niño.

The equatorial west wind anomalies in Fig. 1 appear to branch north, spearhead toward the northeast, passing Hawaii, and aiming at San Francisco. This anomalous surface flow, often know as the "pineapple express", is part of the anomalous cyclonic flow around an anomalous low-pressure system in the North Pacific. The actual wind field bears strong similarly to the anomalies. In the extratropical open ocean, the variation of surface temperature is largely governed by surface heat flux. Winds coming from the tropical ocean bring heat and moisture; they suppress evaporative cooling. The associated clouds may also block solar heating. The opposite is true for winds from the north. This may be the cause of the persistent (over a year) dipoles of SST anomalies in the midlatitude

Pacific, which is visited by cyclones and anticyclones. In May, the warm part of the dipole, with SST anomalies greater than 3°C touched the coast of the U.S.

Figs. 2d, 2e, and 2f show the time-longitude sections, between 30°N and 35°N, extending from the date-line to the Californian coast. In Fig. 2d, winds blowing from south to north are positive (green, yellow, and red) and winds blowing from north to south are negative (blue and purple). The position and zonal movement of the dipole of SST anomalies (Fig. 2e) agree quite well with those of the meridional wind component (Fig. 2d) and surface humidity (Fig 2f). Increase (decrease) in surface humidity will decrease (increase) evaporative cooling of the ocean. Strong southerly winds near the coast in December-January 1996, April-May 1997, and August 1997 coincide with the approach of the SST and surface humidity anomalies toward the coast.

SST anomalies of 1°C are also observed off the coast of Mexico (Fig. 1). As part of the anomalous cyclonic flow in the central Pacific, southerly wind anomalies are found along the coast of Mexico. Fig. 3 shows that the anomalies of subtropical coastal temperature follow approximately the along-shore component of wind. The correlation coefficient of 54 pairs of weekly averaged data is 0.67. Under normal conditions, the subtropical high-pressure system off the coast, with northerly winds along the shore, will cause off shore Ekman transport and coastal upwelling of cold water [Hicky, 1979]. In May 1997, the subtropical high was displaced by a low-pressure system and the associated southerly winds; coastal upwelling was suppressed and warm anomalies appeared.

A strong relationship between equatorial anomalous warming during an El Niño and anomalous warming along the North American coast has been observed [e.g., Simpson et al., 1983]. Atmospheric teleconnection has been postulated as the mechanism that links the equatorial and midlatitude anomalies; the intensification of the Aleutian low pressure system during El Niño has been observed [e.g., Emery and Hamilton, 1985]. Although it is not the intention of this study, with data of limited duration, to unravel the mechanism of teleconnection related to El Niño, the spacebased data used in this study reveal that both the equatorial warming and North American coastal warming are related to wind. The correspondence of the episodes of westerly wind anomalies in the central equatorial Pacific (2a) and the southerly winds off the North American coast (2e) suggests that the wind-forcings of the equatorial and midlatitude thermal anomalies are also related.

Acknowledgment

This study was performed at the Jet Propulsion Laboratory, California Institute of Technology, under contract with the National Aeronautics and Space Administration (NASA). It was jointly supported by the NASA Scatterometer Project, the Earth Observing System Interdisciplinary Science and the Physical Oceanography Programs of NASA.

References

Atlas, R., S.C. Bloom, R.N. Hoffman, J. Ardizzone, and G. Brin, Space-based surface wind vectors to aid understanding of air-sea interaction, *Eos Trans. AGU, 72*, 201-204-205, 208, 1991.

Emery, W.J., and K. Hamilton, Atmospheric forcing of interannual variability in the northeast Pacific Ocean: connections with El Niño, *J. Geophys. Res., 90*, 857-868, 1985.

Hickey, B.M., The California Current system - hypotheses and facts. *Prog. Oceanogr., 8*, 191-279, 1979.

Liu, W.T., W. Tang, and L.L. Fu, Recent warming event in the Pacific may be an El Nino, *Eos Trans. AGU, 76*, 429 &437, 1995

Liu, W.T., W. Tang, and P.P. Niiler, Humidity profiles over the ocean, *J. Climate, 4*, 1023-1034.

Liu, W.T., W. Tang, and P.S. Polito, NASA scatterometer provides global ocean-surface wind fields with more structures than numerical weather prediction, *Geophysical Res. Lett., ,25*, 761-764, 1998

Reynolds R.W., and T. M. Smith, Improved global sea surface temperature analyses using optimum interpolation, *J. Climate, 7*, 929-948, 1994.

Simpson, J.J., Large-scale thermal anomalies in the California Current during the 1982-1983 El Niño, *Geophys. Res. Lett., 10*, 917-940, 1983.

Wentz, F.J., A well-calibrated ocean algorithm for special sensor microwave/imager, *J. Geophys. Res., 102*, 8703-8718, 1997.

List of Figures

Fig. 1 The surface wind anomalies (white arrows) are superimposed on the color map of SST anomalies. Surface winds are derived from NSCAT, and SST is derived from observations of the Advanced Very High Resolution Radiometer blended with in situ measurements [Reynolds and Smith, 1994]. The data are averaged over the period from 22 to 31 of May, 1997. The climatological means for this period of the year have been removed from the two parameters. The climatological mean of SST is derived from the same data set between 1982 and 1996. Since NSCAT was in operation for less than a year, the winds at 10 m height from the European Center for Medium Range Forecasts averaged between 1986 and 1995 were used as climatology.

Fig 2 Time-longitude variation of the interannual anomalies between 2°N and 2°S of (a) zonal component of winds, (b) sea level, and (c) SST. The time-longitude variation of interannual anomalies between 30°N and 35°N of (d) meridional component of surface wind, (e) SST, and (f) surface humidity. After the failure of NSCAT at the end of June 1997, surface winds derived from the Special Sensor Microwave Imager (SSMI) [Atlas et al., 1991] are used. Surface humidity is derived from SSMI integrated water vapor [Liu et al., 1991]. The climatologies of wind and SST are the same as those used in Fig. 1. For sea level and surface humidity, the climatologies are derived from the same sets of data for the periods 1992-1997 and 1991-1996 respectively. The time scales start at the middle of the month.

Fig 3 Temporal variations of the component of surface wind parallel to the coast derived from NSCAT and SST averaged between 15°N and 30°N. The climatological means have been removed.

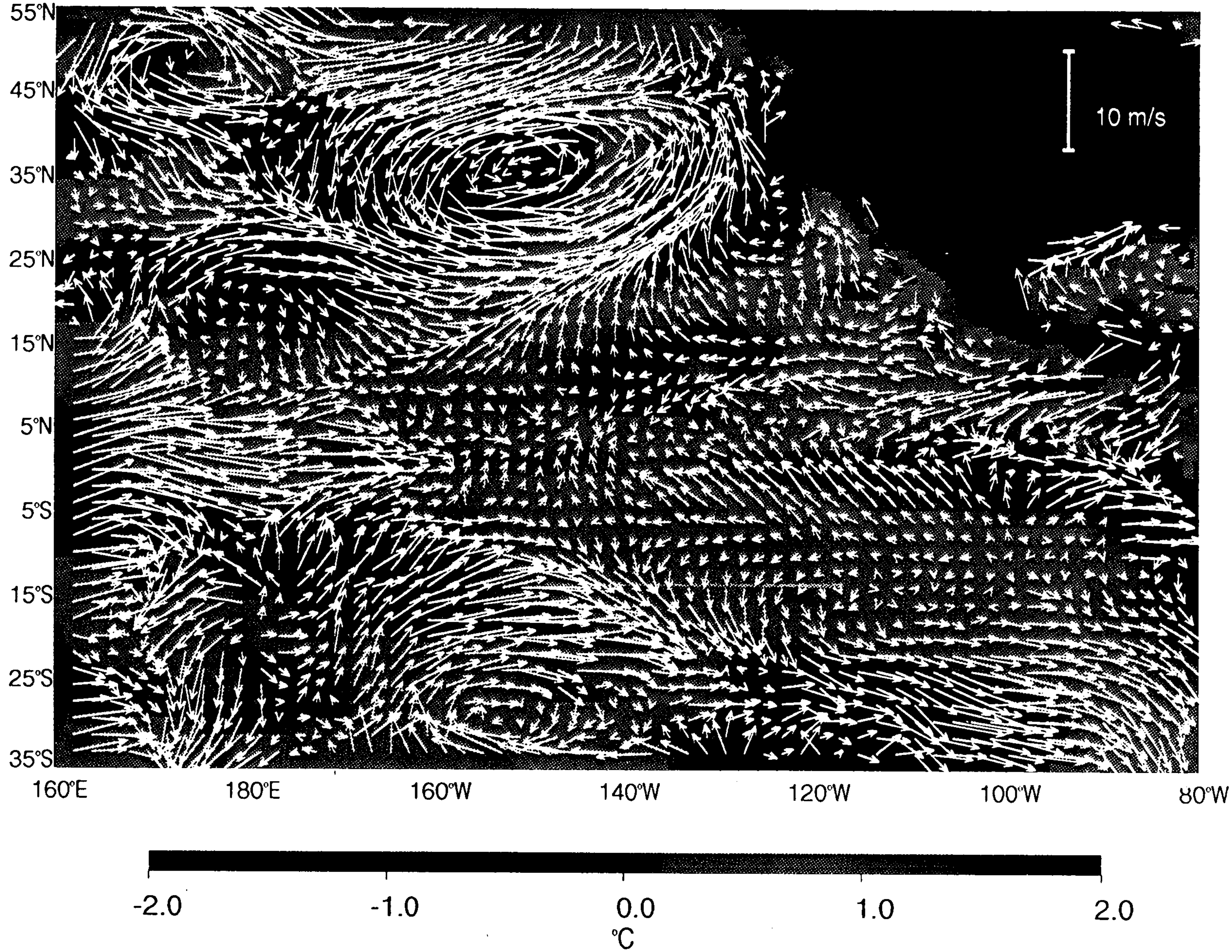
55°N
45°N
35°N
25°N
15°N
5°N
5°S
15°S
25°S
35°S
160°E
180°E
160°W
140°W
120°W
100°W
80°W
10 m/s
-2.0
-1.0
0.0
1.0
2.0
°C

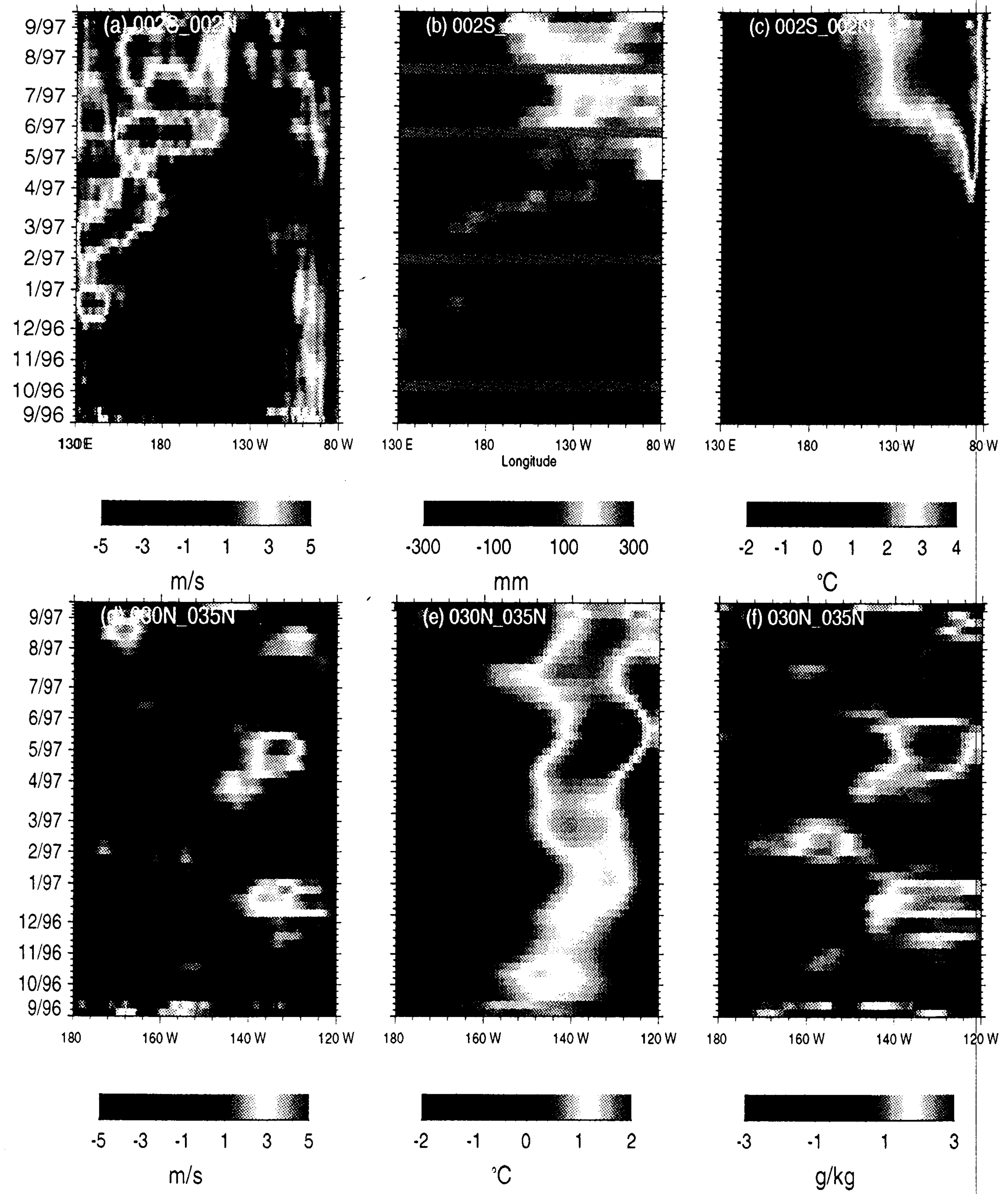

(a) 002S_002N
(b) 002S_
(c) 002S_002N
9/97
8/97
7/97
6/97
5/97
4/97
3/97
2/97
1/97
12/96
11/96
10/96
9/96
130 E
180
130 W
80 W
Longitude
-5 -3 -1 1 3 5
m/s
-300 -100 100 300
mm
-2 -1 0 1 2 3 4
°C
(d) 030N_035N
(e) 030N_035N
(f) 030N_035N
180
160 W
140 W
120 W
-5 -3 -1 1 3 5
m/s
-2 -1 0 1 2
°C
-3 -1 1 3
g/kg